

## Theory of controlling stochastic resonance

Markus Löcher,<sup>1</sup> Mario E. Inchiosa,<sup>2</sup> Joseph Neff,<sup>1</sup> Adi Bulsara,<sup>2</sup> Kurt Wiesenfeld,<sup>1</sup> Luca Gamaitoni,<sup>3</sup>  
Peter Hänggi,<sup>4</sup> and William Ditto<sup>1</sup>

<sup>1</sup>*School of Physics, Georgia Institute of Technology, Atlanta, Georgia 30332-0430*

<sup>2</sup>*Space and Naval Warfare Systems Center, San Diego, Code D-364, San Diego, California 92152-5001*

<sup>3</sup>*Dipartimento di Fisica, Università di Perugia, and Istituto Nazionale di Fisica Nucleare, Sezione di Perugia, I-06100 Perugia, Italy*

<sup>4</sup>*Institut für Physik, Universität Augsburg, Lehrstuhl für Theoretische Physik I, D-86135 Augsburg, Germany*

(Received 9 September 1999; revised manuscript received 19 January 2000)

The concept of *controlling stochastic resonance* has been recently introduced [L. Gamaitoni *et al.*, Phys. Rev. Lett. **82**, 4574 (1999)] to enhance or suppress the spectral response to threshold-crossing events triggered by a time-periodic signal in background noise. Here, we develop a general theoretical framework, based on a rate equation approach. This generic two-state theory captures the essential features observed in our experiments and numerical simulations.

PACS number(s): 05.40.-a, 02.50.Ey, 47.20.Ky, 85.25.Dq

### I. INTRODUCTION

Stochastic resonance (SR) is a nonlinear noise-mediated cooperative phenomenon wherein the coherent response to a deterministic signal can be enhanced in the presence of an optimal amount of noise. Since its inception in 1981 [1], SR has been demonstrated in diverse systems, including sensory neurons, mammalian neuronal tissue, lasers, Superconducting quantum interference devices (SQUIDs), tunnel diodes, and communications devices [2]. Variations and extensions of the classical definition of SR have also appeared in the literature, in connection with systems having nonperiodic inputs (e.g., dc, wideband) with the detector response quantified by various information-theoretic [3] or spectral cross-correlation [4] measures.

Recently, we introduced a control scheme which allows us to enhance or suppress the spectral response in the basic SR effect [5]. Our control strategy is applicable when input information is transmitted via the crossing of either a threshold or potential energy barrier. This raises the intriguing possibility that in situations where external signals might be potentially deleterious, e.g., electromagnetic field interactions with neuronal tissue [6], their effects could be substantially reduced or even eliminated via (externally applied) control signals.

In this work we present a detailed theoretical treatment of the control phenomenon, based on a perturbation-theoretic development of the response power spectral density for weak input signals and weak barrier modulation amplitudes. We focus on the effect of the barrier modulation (the “control”) on the output signal power attenuation and amplification *at the fundamental of the signal frequency*. First, however, we summarize (for the sake of completeness) the recent phenomenological description of the response [5], based on the results of experiments carried out on one of the simplest hysteretic bistable devices, the Schmitt trigger.

### II. PHENOMENOLOGY OF CONTROLLED SR

The motivation for this investigation was the observed rich phenomenology created by the interplay of the two driv-

ing frequencies as seen in the output power spectral densities (PSDs) of a driven Schmitt trigger (ST). Specifically, for relatively large barrier modulation amplitudes, *digital simulations* of the ST reveal “dips” and peaks in the power spectra at combination tones  $|m_1\omega_S \pm m_2\omega_M|$ , with  $\omega_{S,M}$  being the signal and barrier frequencies and  $m_{1,2}$  integers. The phase offset  $\phi$  between the signal and the barrier modulation, as well as the ratio of the frequencies, appear to determine the locations of the peaks and dips, with the height (or depth) determined by the modulation amplitudes. This behavior is depicted in Figs. 1–4. Figures 1 and 2 show two PSDs for  $\omega_M = \omega_S$  and phases  $\phi = 0$  and  $\phi = \pi/2$ , respectively. For small signal but relatively strong barrier modulation, well-defined dips at the even and odd harmonics are evident in the PSD for  $\phi = 0$ . Note that the signal and barrier modulation amplitudes are always taken to be less than the barrier separation  $b$ , so that there are no transitions in the absence of noise. Shifting the phase to  $\pi/2$  results in strong peaks embedded within the same dips, as displayed in Fig. 2. For double frequency modulation  $\omega_M = 2\omega_S$  and phase  $\phi$

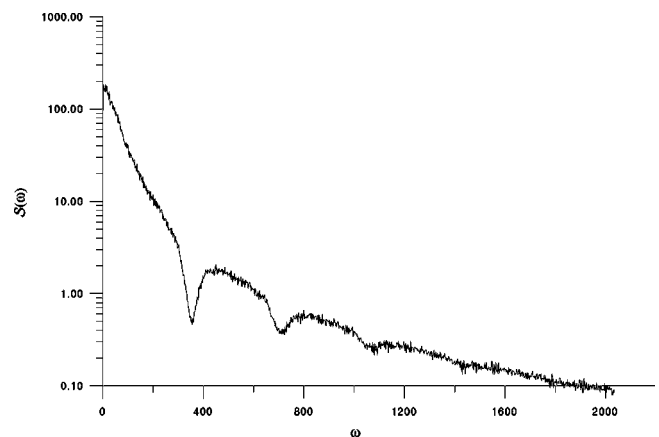
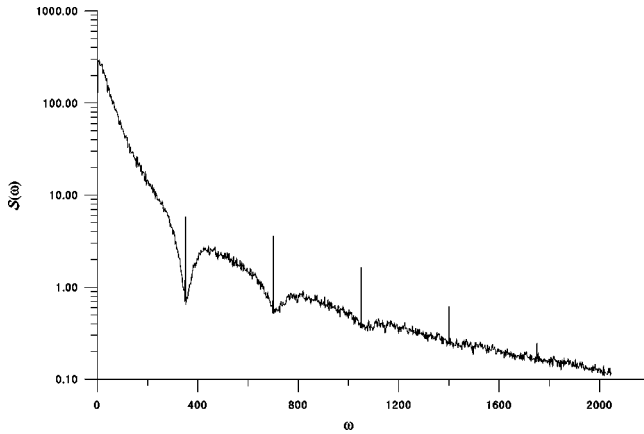
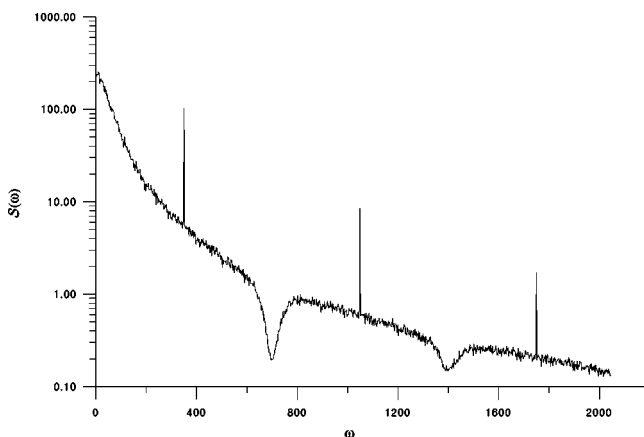
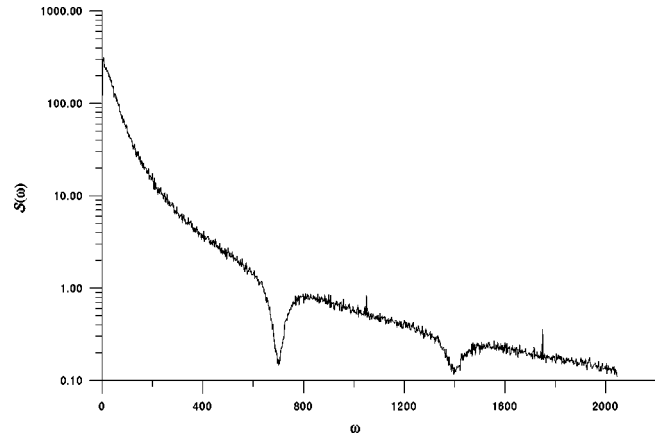


FIG. 1. The power spectral density  $\mathcal{S}(\omega)$  from a numerical simulation of the Schmitt trigger shows dips for equal frequency modulation  $\omega_M = \omega_S$  and phase  $\phi = 0$ . Details of the simulations are described later in the paper; the data shown correspond to parameter values  $\eta_S = 30$ ,  $\eta_M = 200$ ,  $b = 300$ ,  $\sigma = 70$ ,  $\omega_M = 350$ .

FIG. 2. Same as Fig. 1 but with phase  $\phi = \pi/2$ .

$=0$ , the power spectrum in Fig. 3 displays sharp peaks at odd multiples and dips at even multiples of the fundamental frequency  $\omega_S$  (i.e., the dips occur at integer multiples of  $\omega_M$ ). For  $\phi = \pi/2$ , the signal peaks are *suppressed* (Fig. 4). An exploration of all the observed features in the output PSDs is beyond the scope of this work. Instead, following a summarization of the experimental results, the remainder of the paper is aimed at reproducing the experimental results for the signal output power at the fundamental frequency, for the special (and somewhat limited) case of small signal and barrier modulation amplitudes via a perturbation development. Hence, the theory cannot reproduce all the features of the numerically generated (using relatively strong barrier modulation amplitudes) Figs. 1–4.

The experiments were carried out in a modified ST electronic circuit, schematically shown in Fig. 5. The ST is a simple threshold system [7,8] possessing a static hysteretic nonlinearity. The upper and lower threshold voltages are  $V_U = b$  and  $V_L = -b$ , so that  $2b$  is the (static) threshold separation. A subthreshold 64 Hz time-sinusoidal signal  $S(t) = A_S \sin \omega_S t$  ( $A_S < b$ ) and Gaussian noise (band limited at 10 kHz and ac coupled to the ST) are applied to the input. Then, in the absence of any barrier modulation, the standard SR effect can be reproduced at the output of the ST, matching the results of earlier experiments [7] and rate theories [8]. The measured quantity is the output signal power (SP) at the fundamental frequency  $\omega_S$  as a function of input noise

FIG. 3. Same as Fig. 1 but with  $\omega_S = \frac{1}{2} \omega_M$ .FIG. 4. Same as Fig. 3 but with  $\phi = \pi/2$ .

power. Here, the SP is defined as the spectral power at the fundamental frequency  $\omega_S$  (which was taken to be 64 Hz) minus the continuous noise background power within a small frequency range around  $\omega_S$ ; it is, thus, a measure of the height of the signal feature above the noise background in the output PSD.

To realize the control scheme we modulate the upper and lower thresholds sinusoidally,  $V_U(t) = b + A_M \sin(\omega_M t + \phi)$ ,  $V_L(t) = -V_U(t)$ , which results in a “breathing” oscillation (Figs. 6 and 7) of the barriers with frequency  $\omega_M$ . We keep the signal and threshold modulating amplitudes fixed such that  $A_M + A_S < b$  (no deterministic switching) and investigate the system’s response as a function of the phase offset  $\phi$ , which is chosen to be the “control parameter” and the input noise power.

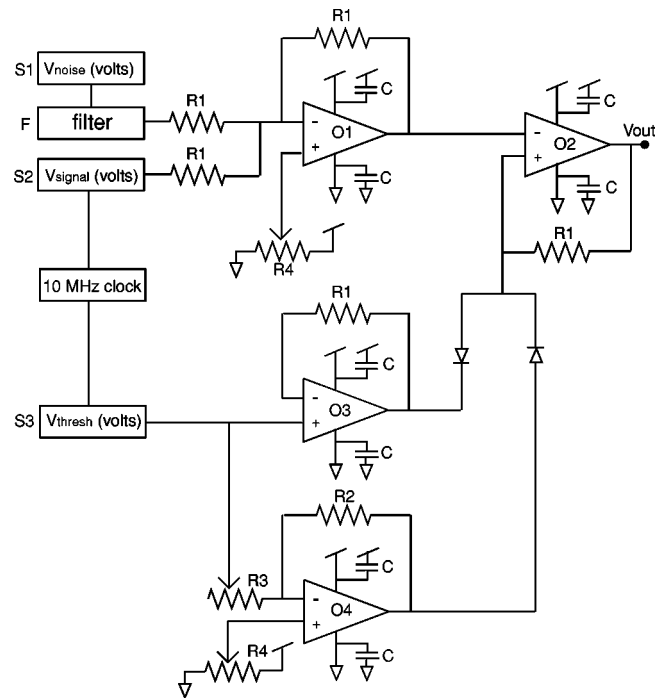


FIG. 5. Circuit diagram for the modified Schmitt trigger. S1, S2, S3: Stanford Research DS345 function generators. F: Stanford Research SR560 preamplifier. O1, O2, O3, O4: Burr-Brown operational amplifiers. The resistor values are  $R_1 = 1 \text{ k}\Omega$ ,  $R_2 = 5 \text{ k}\Omega$ ,  $R_3 = 10 \text{ k}\Omega$ ,  $R_4 = 100 \text{ k}\Omega$ .

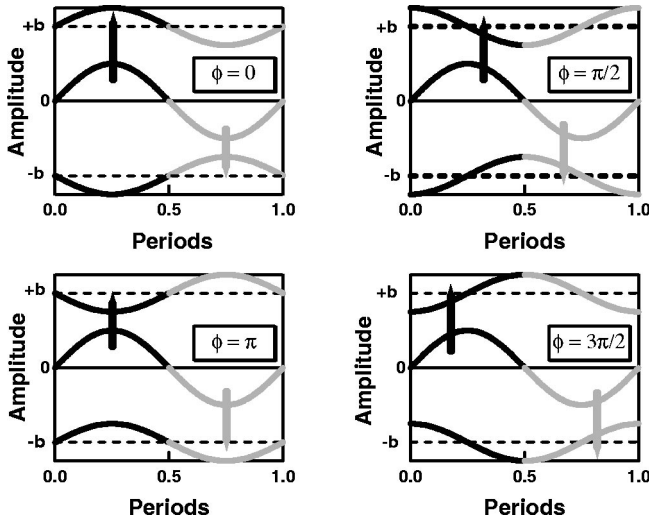


FIG. 6. The input signal  $S(t)$  (middle trace) relative to the modulated upper and lower thresholds, for four different phases. The two frequencies are identical:  $\omega_M = \omega_S$ . Black and gray distinguish the first and second halves of the drive cycle. The arrows indicate the most likely times of switching events.

Our experimental results, first presented in [5], are shown in the gray-scale plots of Fig. 8, where the signal power is gray-scale encoded as a function of the phase and input noise. Analogous results are obtained if the output signal-to-noise ratio is taken as the measure of the response. Figure 8(a) is simply the classic SR case [2] with no control ( $A_M = 0$ ): the signal power passes through a maximum at an optimal noise intensity, with the location of the maximum depending on the internal parameters, as well as the input signal amplitude  $A_S$ , but only weakly on the signal frequency  $\omega_S$ , provided this frequency lies well within the device bandwidth.

Figures 8(b) and 8(c) correspond to the modulated-threshold cases  $\omega_M = \omega_S$ , and  $\omega_M = 2\omega_S$ , respectively. The most striking feature of Fig. 8(b) is a significant *suppression* of the output signal power below its value in the nonmodulated case [Fig. 8(a)], at values 0 and  $\pi$  of the control phase  $\phi$ . Note also that the plot appears symmetric with respect to

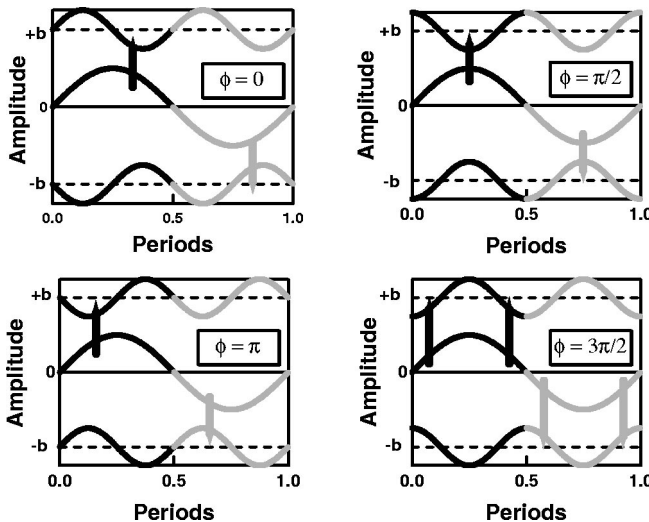


FIG. 7. Same as Fig. 6, but with  $\omega_M = 2\omega_S$ .

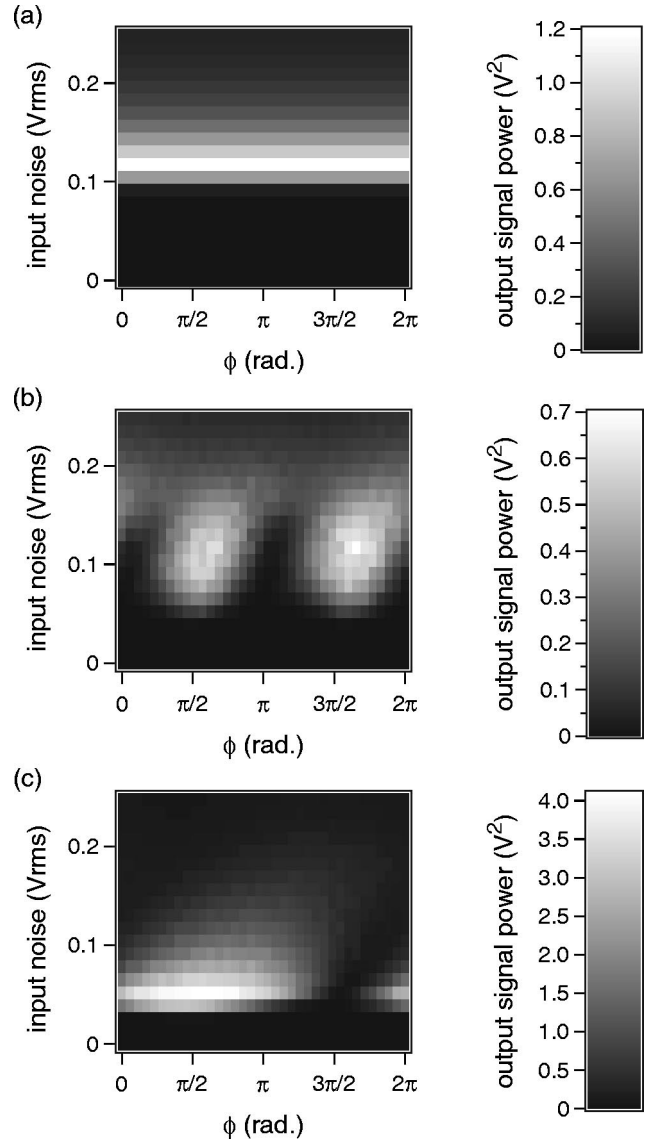


FIG. 8. Experimental results: Gray-scale plot of signal power at  $\omega_S$  vs phase and noise for (a) no modulation, (b)  $\omega_M = \omega_S$ , and (c)  $\omega_M = 2\omega_S$ . Parameters:  $\omega_S = 2\pi 64s^{-1}$ ,  $b = 300$  mV,  $A_M = 200$  mV,  $A_S = 30$  mV. In (b), the maximum signal enhancement occurs near  $\phi = \pi/2$  and  $\phi = 3\pi/2$ , and the maximum suppression occurs near phases  $\phi = 0$  and  $\phi = \pi$ . In (c), the maximum signal enhancement occurs near  $\phi = \pi/2$ , and the maximum suppression occurs near  $\phi = 3\pi/2$ . Note the differing signal power gray scales in (a), (b), and (c).

a phase translation of  $\pi$ . A suppression behavior is also present in the case where  $\omega_M = 2\omega_S$  for  $\phi = 3\pi/2$  [Fig. 8(c)]; however, in this case, a significant enhancement of the output SP (compared to the nonmodulated case) is also evident at phase  $\phi = \pi/2$ .

The principle goal of this paper is to achieve a quantitative understanding of the suppression and enhancement effects for each of the two modulation schemes. In Sec. III we derive expressions for the output power at the signal frequency, first for double frequency modulation, then for equal frequency modulation. Though straightforward, these calculations are not trivial: they need to be taken to cubic and quartic order, respectively, in order to capture the key effects of controlled SR. In Sec. IV we test these analytic predic-

tions against numerical simulations of three different bistable systems. Taken together, our results demonstrate that controlled SR is a generic phenomenon for such systems, and can be understood in a unified way.

Our control scheme, which is implemented via modulation of the potential energy barrier by a time-sinusoidal signal with controlled phase, must be contrasted to the case of multiple cyclic inputs applied at the input of a nonlinear device. In this case, one obtains ‘‘combination tones’’ at frequencies  $|n_1\omega_1 \pm n_2\omega_2|$  (for two input signals of frequency  $\omega_{1,2}$ ) with  $n_{1,2}$  being integers and the symmetry of the system setting selection rules for the appearance of specific sets of combination tones in the response. This case was already discussed in the 19th century by von Helmholtz [9] in connection with frequency mixing in the inner ear. With noise, one observes [10] a SR effect at every combination tone that appears in the output, with the symmetry of the device once again predicating the appearance of certain sets of frequencies in the output PSD.

### III. GENERAL THEORY

We consider a two-state system. We have in mind a fairly general bistable system, but it will be conceptually convenient sometimes to use language specific to the Schmitt trigger. The two states correspond to output values  $+c$  and  $-c$ , respectively. For convenience, we will also refer to the states themselves as  $\pm c$ . Following Ref. [8], we suppose that the dynamics is governed by rate equations for the state probabilities  $p_{\pm}$  that the system is in the state  $\pm c$ ,

$$\dot{p}_+ = W_-(t)p_- - W_+(t)p_+ = -\dot{p}_-, \quad (1)$$

where  $W_{\pm}(t)$  is the transition rate *out of* the  $\pm$  state, and the overdot denotes differentiation with respect to time. In the modulation schemes we are considering, the transition rates are time periodic. The solution to the linear first-order differential equation (1) is

$$p_+(t) = \frac{1}{g(t)} \left[ p_+(t_0)g(t_0) + \int_{t_0}^t W_-(t')g(t')dt' \right], \quad (2)$$

where

$$g(t) = \exp \int [W_+(t) + W_-(t)]dt. \quad (3)$$

Replacing  $p_+(t_0)$  in Eq. (2) with  $\delta_{x_0c}$  gives us the conditional probability  $p_+(t|x_0, t_0)$  that the system at time  $t$  is in the  $+c$  state given that the state at time  $t_0$  was  $x_0$  (which may be  $+c$  or  $-c$ ):

$$p_+(t|x_0, t_0) = \frac{1}{g(t)} \left[ \delta_{x_0c}g(t_0) + \int_{t_0}^t W_-(t')g(t')dt' \right]. \quad (4)$$

The conditional probability density of the two-state output  $x(t)$  is

$$\begin{aligned} p(x, t|x_0, t_0) &= p_+(t|x_0, t_0)\delta(x-c) + p_-(t|x_0, t_0)\delta(x+c) \\ &= p_+(t|x_0, t_0)\delta(x-c) + [1 - p_+(t|x_0, t_0)] \\ &\quad \times \delta(x+c). \end{aligned} \quad (5)$$

The conditional expectation value is

$$\langle x(t)|x_0, t_0 \rangle = \int_{-\infty}^{\infty} xp(x, t|x_0, t_0)dx = c[2p_+(t|x_0, t_0) - 1]. \quad (6)$$

To focus on generic behavior, independent of initial conditions, we form the *asymptotic* expectation value  $\langle x(t) \rangle_{\text{as}}$

$$\langle x(t) \rangle_{\text{as}} \equiv \lim_{t_0 \rightarrow -\infty} \langle x(t)|x_0, t_0 \rangle = c[2p_+^{\text{as}}(t) - 1], \quad (7)$$

where  $p_+^{\text{as}}(t) \equiv p_+(t|x_0, t_0 \rightarrow -\infty)$ .

To calculate  $p_+^{\text{as}}(t)$ , notice that the initial condition term in Eq. (4) can be rewritten in terms of a definite integral,

$$\delta_{x_0c} \frac{g(t_0)}{g(t)} = \delta_{x_0c} \exp \left\{ - \int_{t_0}^t [W_+(t') + W_-(t')]dt' \right\}. \quad (8)$$

Since the rates  $W_{\pm}$  may be assumed to be bounded from below by a positive constant, the integral in Eq. (8) will approach  $+\infty$  as  $t_0 \rightarrow -\infty$ , and the initial condition term (8) will decay exponentially, yielding

$$p_+^{\text{as}}(t) = \frac{1}{g(t)} \int_{-\infty}^t W_-(t')g(t')dt'. \quad (9)$$

We assume that in the adiabatic limit (where the signal and modulation frequencies  $\omega_{S,M}$  are well within the trigger and noise bandwidths), the rates are given by

$$W_{\pm}(t) = f[\mu \pm \eta_S \sin \omega_S t + \eta_M \sin(\omega_M t + \phi)], \quad (10)$$

where, in general, the specific form of  $f$  would depend on the system being investigated. The parameters  $\mu$  and  $\eta_{S,M}$  correspond to the threshold  $b$  and signal/modulation amplitudes scaled by the noise power (referred to  $D$  or  $\sigma$  in the following sections).

Assuming the typical experimental case in which the starting times from run to run are random with respect to the signal and modulation phases, it is appropriate to average the correlation function over the initial phases. Alternatively, we can avoid adding another phase variable to Eq. (10) by cycle averaging the correlation function over  $t$ . Here, one cycle is defined as the period of  $W_{\pm}(t)$ , so we restrict ourselves to cases where  $\omega_S$  and  $\omega_M$  are commensurate frequencies.

Cycle averaging over  $t$  yields a stationary correlation function  $\bar{K}(\tau)$ . Taking the longtime limit  $\tau \rightarrow \infty$  eliminates time-decaying correlations (noise background) while preserving correlations that persist indefinitely (signal) [11]. The resulting initial-phase-averaged asymptotic correlation function  $\bar{K}_{\text{as}}(\tau)$  can be written in terms of the asymptotic expectation value (7) (see Gammaitoni *et al.* in [2]),

$$\begin{aligned}\bar{K}_{\text{as}}(\tau) &= \langle\langle x(t+\tau) \rangle_{\text{as}} \langle x(t) \rangle_{\text{as}} \rangle_t \\ &= \langle c^2 [2p_+^{\text{as}}(t+\tau) - 1][2p_+^{\text{as}}(t) - 1] \rangle_t, \quad (11)\end{aligned}$$

where  $\langle \cdot \rangle_t$  denotes a cycle average over  $t$ . Fourier transforming  $\bar{K}_{\text{as}}(\tau)$  will lead to a formula for the total output power at the signal frequency  $\omega_S$ .

For small signal and threshold modulation  $\eta_{S,M} \ll 1$ , we can expand the rates  $W_{\pm}(t)$  in  $\eta_{S,M}$ ,

$$\begin{aligned}W_{\pm}(t) &= \frac{1}{2} \sum_{n=0}^{\infty} (-1)^n \alpha_n [\pm \eta_S \sin(\omega_S t) \\ &\quad + \eta_M \sin(\omega_M t + \phi)]^n. \quad (12)\end{aligned}$$

Here, the  $\alpha_n$  are the expansion coefficients  $\alpha_n = [2(-1)^n/n!][d^n f(\mu)/d\mu^n]$  [the factor  $(-1)^n$  is included to keep  $\alpha_1$  positive]. For any specific example these coefficients are found via a formal expansion of the transition rates  $W_{\pm}$ . For the Schmitt trigger, these rates can be cast as the inverses of the mean first passage times of a Brownian particle to an absorbing barrier at the switching threshold [8], provided the noise bandwidth is within that of the device.

We can compute  $p_+^{\text{as}}(t)$  to  $n$ th order as follows. We use Eq. (12) to obtain the rates expanded to  $n$ th order. We insert the expanded rates into Eq. (3) and Taylor expand the exponential to obtain an expansion of  $g(t)$  to  $n$ th order. We multiply the  $n$ th order expansions of  $W_-(t)$  and  $g(t)$ , discard terms above  $n$ th order, and integrate to obtain the expansion of  $\int_{-\infty}^t W_-(t')g(t')dt'$ . We multiply the result by the  $n$ th order expansion of  $1/g(t)$  and discard higher order terms to obtain the desired expansion of  $p_+^{\text{as}}(t)$  to  $n$ th order.

Having obtained an expansion of  $p_+^{\text{as}}(t)$  to  $n$ th order, one can use Eq. (11) to obtain an expansion of the asymptotic correlation function, but to what order is it correct? First, note that in the unmodulated case ( $\eta_{S,M}=0$ ) the rates  $W_{\pm}$  are equal, implying  $p_+^{\text{as}}(t)=1/2$ . This implies that in an expansion of  $2p_+^{\text{as}}(t)-1$ , the lowest order term is of at least first order in  $\eta_{S,M}$ . It follows that an  $n$ th order expansion of  $p_+^{\text{as}}(t)$  will give us an asymptotic correlation function (11) with a leading order of at least 2. Also, the asymptotic correlation function will be correct to (at least) order  $n+1$ .

### A. Double frequency modulation

At this stage in the calculation we specify the barrier modulation frequency  $\omega_M$ . We will begin with the case  $\omega_M=2\omega_S$ ; in Sec. III B we will turn to the case of equal frequency modulation.

It turns out that the required calculations are rather involved, because to attain a sufficiently accurate and consistent final result [Eq. (17) below], we have to keep terms through cubic order in the expansion (12). As a result, the expressions for the intermediate steps are very long, which unfortunately tends to obscure the essential structure of the derivation. Therefore, for the sake of clarity we present here the calculation of the power spectrum in which we truncate the expansion (12) after its quadratic term. We then simply quote the final result of the derivation which keeps the higher order terms. The interested reader can find full details of the latter derivation on AIP's Electronic Physics Auxiliary Publication Service (EPAPS) [13].

Following the procedure outlined in Sec. II, we find Eq. (9) to quadratic order in  $(\eta_S, \eta_M)$

$$\begin{aligned}p_+^{\text{as}}(t) &= \frac{1}{2} + \frac{\alpha_1 \eta_S [-\omega_S \cos(\omega_S t) + \alpha_0 \sin(\omega_S t)]}{2(\alpha_0^2 + \omega_S^2)} - \eta_S \eta_M \left[ \frac{(\alpha_0 2\alpha_2 - \alpha_1^2) \cos(\omega_S t + \phi) + 2\alpha_2 \omega_S \sin(\omega_S t + \phi)}{4(\alpha_0^2 + \omega_S^2)} \right. \\ &\quad \left. + \frac{1}{8} \left( \frac{-\alpha_1^2}{\alpha_0^2 + \omega_S^2} + \frac{2\alpha_0 2\alpha_2 - 3\alpha_1^2}{\alpha_0^2 + 9\omega_S^2} \right) \cos(3\omega_S t + \phi) + \frac{\omega_S (6\alpha_0^2 \alpha_2 + 6\alpha_2 \omega_S^2 - 4\alpha_0 \alpha_1^2)}{4(\alpha_0^2 + \omega_S^2)(\alpha_0^2 + 9\omega_S^2)} \sin(3\omega_S t + \phi) \right]. \quad (13)\end{aligned}$$

Since  $p_+^{\text{as}}(t)$  was expanded to quadratic order,  $\langle x(t+\tau) \rangle_{\text{as}} \langle x(t) \rangle_{\text{as}}$  is correct through third order,

$$\langle x(t+\tau) \rangle_{\text{as}} \langle x(t) \rangle_{\text{as}} = \frac{c^2 \alpha_1^2 \eta_S^2}{2(\alpha_0^2 + \omega_S^2)} \left( 1 - \eta_M \frac{\alpha_1^2 \omega_S \cos(\phi) - (\alpha_0^2 2\alpha_2 - \alpha_0 \alpha_1^2 + 2\alpha_2 \omega_S^2) \sin(\phi)}{\alpha_1(\alpha_0^2 + \omega_S^2)} \right) \cos(\omega_S \tau) + \dots \quad (14)$$

plus a multitude of  $t$ -dependent terms of the form  $\cos$  or  $\sin(N\omega_S t + \dots)$ , where  $N$  is a nonzero integer. None of these terms will survive the process of cycle averaging over  $t$  that yields the initial-phase-averaged asymptotic correlation function  $\bar{K}_{\text{as}}(\tau) = \langle\langle x(t+\tau) \rangle_{\text{as}} \langle x(t) \rangle_{\text{as}} \rangle_t$ .

From the coefficient of  $\delta(\omega - \omega_S)$  in the (one-sided) power spectrum  $2\int_{-\infty}^{\infty} \bar{K}_{\text{as}}(\tau) e^{-i\omega\tau} d\tau$ , we find that the total output power at the signal frequency  $\omega_S$  is

$$\frac{\pi c^2 \alpha_1^2 \eta_S^2}{\alpha_0^2 + \omega_S^2} \left[ 1 - \eta_M \alpha_1 \left\{ \frac{\omega_S \cos \phi + \alpha_0 \sin \phi}{\alpha_0^2 + \omega_S^2} - \frac{2\alpha_2}{\alpha_1^2} \sin \phi \right\} \right] \quad (15)$$

for  $\omega_M=2\omega_S$ . One can rewrite Eq. (15) in the following manner:

$$\frac{\pi c^2 \alpha_1^2 \eta_S^2}{\alpha_0^2 + \omega_S^2} \left[ 1 - \eta_M \alpha_1 \left\{ \frac{\sin(\phi + \Theta)}{\sqrt{\alpha_0^2 + \omega_S^2}} - \frac{2\alpha_2}{\alpha_1^2} \sin \phi \right\} \right], \quad (16)$$

with  $\Theta = \tan^{-1}(\omega_S/\alpha_0)$ . As noted earlier,  $\alpha_1$  is a positive coefficient.

The same steps leading to Eq. (15) can be retraced using a less severe truncation of the transition rates  $W_{\pm}(t)$ . As we show later, all the key features of the controlled SR scheme are reproduced if we keep terms through cubic order as indicated in Eq. (12). The details of the derivation can be found elsewhere [13]. The result corresponding to Eq. (15) is

$$\begin{aligned} & \frac{\pi c^2 \alpha_1^2 \eta_S^2}{\alpha_0^2 + \omega_S^2} \left[ 1 - \eta_M \alpha_1 \left( \frac{\omega_S \cos \phi + \alpha_0 \sin \phi}{\alpha_0^2 + \omega_S^2} - \frac{2\alpha_2}{\alpha_1^2} \sin \phi \right) \right. \\ & + \eta_M^2 \left( \frac{\alpha_2^2 + 3\alpha_1 \alpha_3}{\alpha_1^2} + \frac{\alpha_1^2 - 6\alpha_0 \alpha_2}{2(\alpha_0^2 + \omega_S^2)} + \frac{3\alpha_1^2 - 4\alpha_0 \alpha_2}{4\alpha_0^2 + 36\omega_S^2} \right) \\ & \left. + \frac{3}{2} \eta_S^2 \left( \frac{\alpha_3}{\alpha_1} - \frac{\alpha_0 \alpha_2}{\alpha_0^2 + \omega_S^2} \right) \right]. \quad (17) \end{aligned}$$

## B. Equal frequency modulation

We performed analogous calculations as above for the case  $\omega_M = \omega_S$ , which is straightforward but tedious. Here, we present only the final expression for the output power at the signal frequency  $\omega_S$ . The interested reader can find the complete derivation on the Internet [13]. The result is

$$P_{\text{dc}} = \frac{\pi c^2 \eta_M^2 \eta_S^2 [(-\alpha_0 \alpha_1^2 + 2\alpha_0^2 \alpha_2 + 2\alpha_2 \omega_S^2) \cos \phi + \alpha_1^2 \omega_S \sin \phi]^2}{2\alpha_0^2 (\alpha_0^2 + \omega_S^2)^2}. \quad (20)$$

Intuitively, the origin of this effect can be understood by contemplating Fig. 6. There are two contributions. First, we can see that the modulation induces an asymmetry in the two transition rates, keeping in mind that the transitions are much more likely to occur when the barrier distance is smallest (denoted by the two arrows in the figure; we refer the interested reader to the Appendix for a brief discussion on the existence of this minimum distance). For example, when  $\phi = 0$ , the upward transition rate is much smaller than the downward rate, and the reverse is true when  $\phi = \pi$ . This asymmetry leads to the  $\cos \phi$  term in Eq. (20). The second effect, which gives rise to the  $\sin \phi$  contribution, reflects a difference between the time intervals between optimal up-

$$\begin{aligned} & \frac{\pi c^2 \alpha_1^2 \eta_S^2}{\alpha_0^2 + \omega_S^2} \left[ 1 + \eta_M^2 \left\{ \frac{(\alpha_1^2 - \alpha_0 \alpha_2)(\alpha_0 \cos 2\phi - \omega_S \sin 2\phi)}{2\alpha_0(\alpha_0^2 + \omega_S^2)} \right. \right. \\ & - \left. \left( \frac{\alpha_2}{\alpha_0} - \frac{3\alpha_3}{2\alpha_1} \right) \cos 2\phi - \frac{\alpha_2}{\alpha_0} + \frac{3\alpha_3}{\alpha_1} - \frac{\alpha_0 \alpha_2}{\alpha_0^2 + \omega_S^2} \right. \\ & \left. \left. + \frac{\alpha_1^2 - \alpha_0 \alpha_2}{\alpha_0^2 + 4\omega_S^2} \right\} + \frac{3\eta_S^2}{2} \left( \frac{\alpha_3}{\alpha_1} - \frac{\alpha_0 \alpha_2}{\alpha_0^2 + \omega_S^2} \right) \right] \quad (18) \end{aligned}$$

for  $\omega_M = \omega_S$ . We note that the lowest order correction to the signal power is quartic, compared to cubic in the double frequency case. In order to get consistent results to this order, the expansion of the rates (12) has to contain all terms up to and including cubic order. As above, we can introduce the phase  $\Theta = \tan^{-1}(\omega_S/\alpha_0)$  and rewrite Eq. (18) as

$$\begin{aligned} & \frac{\pi c^2 \alpha_1^2 \eta_S^2}{\alpha_0^2 + \omega_S^2} \left[ 1 + \eta_M^2 \left\{ \frac{(\alpha_1^2 - \alpha_0 \alpha_2) \cos(2\phi + \Theta)}{2\alpha_0 \sqrt{\alpha_0^2 + \omega_S^2}} \right. \right. \\ & - \left. \left( \frac{\alpha_2}{\alpha_0} - \frac{3\alpha_3}{2\alpha_1} \right) \cos 2\phi - \frac{\alpha_2}{\alpha_0} + \frac{3\alpha_3}{\alpha_1} - \frac{\alpha_0 \alpha_2}{\alpha_0^2 + \omega_S^2} \right. \\ & \left. \left. + \frac{\alpha_1^2 - \alpha_0 \alpha_2}{\alpha_0^2 + 4\omega_S^2} \right\} + \frac{3\eta_S^2}{2} \left( \frac{\alpha_3}{\alpha_1} - \frac{\alpha_0 \alpha_2}{\alpha_0^2 + \omega_S^2} \right) \right]. \quad (19) \end{aligned}$$

## C. dc symmetry breaking

It is worthwhile emphasizing a unique qualitative feature of the controlled SR scheme. While a traditional SR experiment (i.e., one with no barrier modulation) on a symmetric Schmitt trigger yields zero average dc output, the barrier modulation can break the plus-minus symmetry between the two states and thereby generate a finite dc output power. This effect occurs only for equal frequency modulation. Analytically, the dc term in the power spectrum arises from a  $\tau$ -independent term in the autocorrelation function [13]. The expression for the dc part of the power spectral density ( $\omega_M = \omega_S$ ) is

down and down-up transitions. Again looking at Fig. 6, we see for  $\phi = \pi/2$  that the separation between optimal transition points is significantly different from a half-period, which results in an asymmetric output square wave, and thus a non-zero average (dc) component.

## IV. COMPARISON WITH NUMERICAL SIMULATIONS

### A. Direct simulations of the truncated rate equations

As a first step in testing the analytic predictions, we carried out direct simulations of the time-dependent rate equations. In general, the experimentally measured power spec-

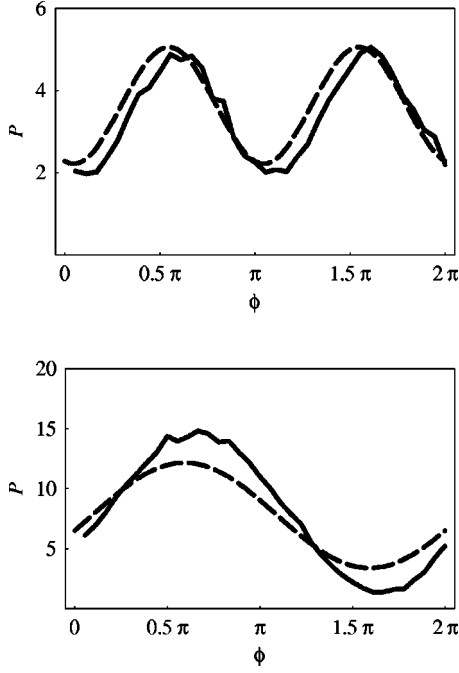


FIG. 9. Output signal power  $P$  vs phase  $\phi$  from direct simulations of the rate equations (12) for  $\omega_M = \omega_S$  (top) and  $\omega_M = 2\omega_S$  (bottom), respectively. The dashed line in each figure is the corresponding theoretical result (18) and (17), respectively. Parameter values are  $\alpha_0 = 0.37174 = \frac{1}{2}\alpha_1 = \frac{1}{2}\alpha_2 = \frac{3}{4}\alpha_3$ ,  $c = 5.66$ ,  $\eta_S = 8c/D$ ,  $\eta_M = 16c/D$ , and  $D = 140$ .

tral density  $S_{\text{expt}}$  relates to the theoretical signal power  $P$  [given by either Eq. (18) or Eq. (17)] in the following manner [8]:

$$S_{\text{expt}} = \frac{PG + N\Delta}{\Delta}.$$

Here,  $\Delta$  is the bin width of the measured power spectral density,  $N$  is the noise background power spectral density at the signal frequency, and  $G$  is the so-called processing gain factor (typically between 0.5 and 1), which is an effect of windowing the time series before Fourier analyzing it. In all subsequent simulations we employed a Welch window with a processing gain  $G = 0.83$ .

In order to check the consistency of our numerical algorithm, we numerically integrated the rate equations as given by Eq. (12), including terms up to fourth order, in the following manner. At each time step a random number  $\xi$  is chosen uniformly on the interval  $[0,1]$ . If the system is currently in the  $\pm$  state,  $\xi$  is compared with  $p_{\pm}(t) = \Delta t W_{\pm}(t)$ , where  $\Delta t$  is the time step. If  $\xi < p_{\pm}$ , the system is changed to the other state [8]. Figure 9 shows a comparison between the theoretical predictions and the results from the rate equation, for the output signal power as a function of the modulation phase. Because of the various approximations in the course of the derivation of Eqs. (18) and (17) we do not expect perfect agreement. Nevertheless, the matching is good enough to strengthen our confidence in the numerical results presented in the subsequent subsections.

## B. The double-well system

It is of interest to test the developed two-state theory for systems with continuous state variables. Here, we consider the simplest bistable dynamic potential

$$U(x) = -\frac{a}{2}x^2 + \frac{b}{4}x^4, \quad (21)$$

where the potential minima are at  $\pm c = \pm\sqrt{a/b}$ , and  $U_0 = a^2/4b$  is the (unmodulated) barrier height. We furthermore consider the limit of large damping and thus assume that the Langevin equation is given by

$$\dot{x} = -\partial_x U(x) + \sqrt{D}\xi(t), \quad (22)$$

where  $\xi(t)$  is  $\delta$ -correlated white noise with unit variance, so that

$$\langle \xi(t)\xi(t') \rangle = \delta(t-t'). \quad (23)$$

We also restrict ourselves to the high-barrier, adiabatic limit, so that we may identify the transition rates  $W_{\pm}$  with the Kramers rate, to a good approximation, which in the absence of modulation is given by

$$W_{\pm} = \frac{\sqrt{U''(0)U''(c)}}{2\pi} \exp[-2U_0/D]. \quad (24)$$

It is worth noting that the Kramers rate is derived under the assumption that the probability density within a well is roughly at equilibrium. That is still the case if the signal frequency is much lower than the rate at which the probability equilibrates, which is simply  $U''(\pm c)$ . Thus we require  $\omega \ll U''(\pm c) = 2a$ . In the vast majority of the SR literature [2,8] the modulation term ( $\sim U_S x \sin \omega_S t$ ) is simply added to the right side of Eq. (21). This has the effect of not only modulating the barrier heights, but also the position of the potential extrema and their curvatures. On the other hand, it is conceptually simpler to modify only the barrier heights, so that the modified Kramers rate becomes

$$W_{\pm}(t) = \frac{a}{\sqrt{2\pi}} \exp\{-2[U_0 \pm U_S \sin \omega_S t + U_M \sin(\omega_M t + \phi)]/D\} \quad (25)$$

Equation (25) is true only to linear order if one merely adds the modulation terms to the potential (21). Here we use an alternative approach which alters the barrier height directly. This has the advantage of giving a consistent path from Eq. (24) to Eq. (25); the disadvantage is that the simpler picture is slightly less elegant algebraically. Since the curvatures  $U''(0) = -a$ ,  $U''(c) = 2a$  do not depend on the parameter  $b$ , it is possible to modulate the barrier height  $a^2/4b$  and keep the curvatures and thus the prefactor in Eq. (24) constant. In order to implement the symmetric barrier modulation and the asymmetric ‘‘rocking’’ of the potential, we allow the barrier height, and thus  $b$ , to depend on  $x$  and  $t$  and to be different on each side of the origin,

$$b \rightarrow b(x,t) = b_+(t) \quad \text{if } x \geq 0 \\ = b_-(t) \quad \text{if } x < 0$$

with

$$\frac{a^2}{4b_{\pm}(t)} = U_0 \pm U_S \sin \omega_S t + U_M \sin(\omega_M t + \phi) \\ \Rightarrow b_{\pm}(t) \\ = \frac{a^2}{4[U_0 \pm U_S \sin \omega_S t + U_M \sin(\omega_M t + \phi)]}. \quad (26)$$

Modulating the coefficient  $b$  from Eq. (21) in such a way guarantees that, within the adiabatic approximation, Eq. (25) is exact. We emphasize that we chose this modulation as a mere technical convenience to avoid further approximations.

Comparing Eqs. (10) and (25), we have  $\mu = U_0/D$ ,  $\eta_S = U_S/D$ ,  $\eta_M = U_M/D$ , and

$$f[\mu \pm \eta_S \sin \omega_S t + \eta_M \sin(\omega_M t + \phi)] \\ = (a/\sqrt{2}\pi) \exp\{-2[\mu \pm \eta_S \sin \omega_S t \\ + \eta_M \sin(\omega_M t + \phi)]\}, \\ \alpha_0 = 2f(\mu) = \frac{\sqrt{2}a}{\pi} \exp(-2U_0/D), \\ \alpha_1 = -2 \left. \frac{df(x)}{dx} \right|_{x=\mu} = \frac{2\sqrt{2}a}{\pi} \exp(-2U_0/D) = 2\alpha_0, \quad (27)$$

$$\alpha_2 = \frac{2}{2!} \left. \frac{d^2 f(x)}{dx^2} \right|_{x=\mu} = \frac{2\sqrt{2}a}{\pi} \exp(-2U_0/D) = \alpha_1, \\ \alpha_3 = \frac{-2}{3!} \left. \frac{d^3 f(x)}{dx^3} \right|_{x=\mu} = \frac{2 \times 8a}{6\sqrt{2}\pi} \exp(-2U_0/D) = \frac{4}{3} \alpha_0.$$

In Fig. 10 we compare the analytical predictions (bottom panels) against numerical simulations (top panels) for the case of double frequency modulation,  $\omega_M = 2\omega_S$ , using ‘‘typical’’ parameter values. The agreement is good. For the case of single frequency modulation,  $\omega_M = \omega_S$ , Fig. 11 shows a similarly good match between the fourth order result (18) and numerical simulations of the double well potential.

As we alluded to in Sec. III C, the average dc output predicted by Eq. (20) can be compared to numerical simulations. This comparison is shown in Fig. 12, where we have plotted the square of the averaged mean value of  $x$ . The agreement is rather good. We also see that the dc output is largest close to phases  $\phi = 0$  and  $\pi$ , which indicates that for this system the  $\cos \phi$  term in Eq. (20) is dominant over the  $\sin \phi$  contribution. It follows that the corresponding physical mechanism reflected in the data is a modulation-induced asymmetry in the up/down transition rates (see the discussion in Sec. III C).

### C. The Schmitt trigger

A dynamical model for the Schmitt trigger was introduced previously [Eq. (6.21) in Ref. [8]]. We can modify that

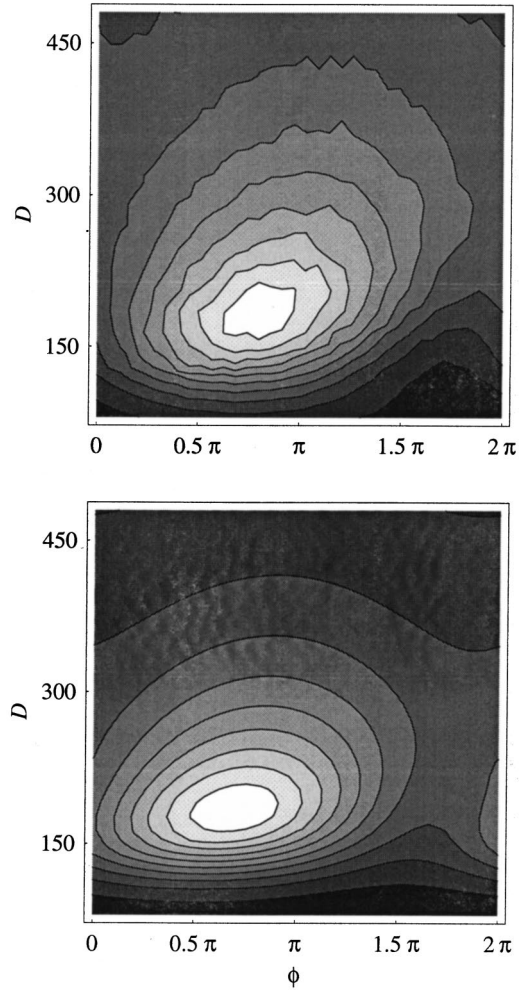


FIG. 10. Output signal power vs input noise strength  $D$  and modulation phase  $\phi$  for the double well system with  $\omega_M = 2\omega_S$ . Top: digital simulations; bottom: the analytical predictions (17). The gray scale range is (0,20). Parameter values are  $U_0 = 256$ ,  $2c = 11.13$ ,  $U_S = 8$ , and  $U_M = 16$

model to fit the present situation by including the threshold modulation in the effective gain  $\tilde{\gamma} = \gamma + \epsilon_M \cos(\omega_M t + \phi)$ ,

$$y = \text{sgn}[\tilde{\gamma}y - \epsilon_S \cos \omega_S t - x],$$

$$\dot{x} = -kx + \sigma \xi(t). \quad (28)$$

Here,  $x$  represents colored noise with correlation time  $\tau_c = k^{-1}$  [ $\xi(t)$  is  $\delta$  correlated white noise with unit variance] so that the variance of  $x$  is  $\langle x^2 \rangle = \sigma^2/2k$ . In order to evaluate the analytic predictions, we need expressions for the expansion coefficients  $\alpha_n$  up to  $n=3$ . We find

$$\frac{\sqrt{\pi}}{k} \alpha_0 = \left( \int_{-\mu}^{\mu} e^{u^2} \phi(u) du \right)^{-1},$$

$$\frac{\sqrt{\pi}}{k} \alpha_1 = \frac{e^{\mu^2} (\phi(\mu) - \phi(-\mu))}{\left( \int_{-\mu}^{\mu} e^{u^2} \phi(u) du \right)^2},$$

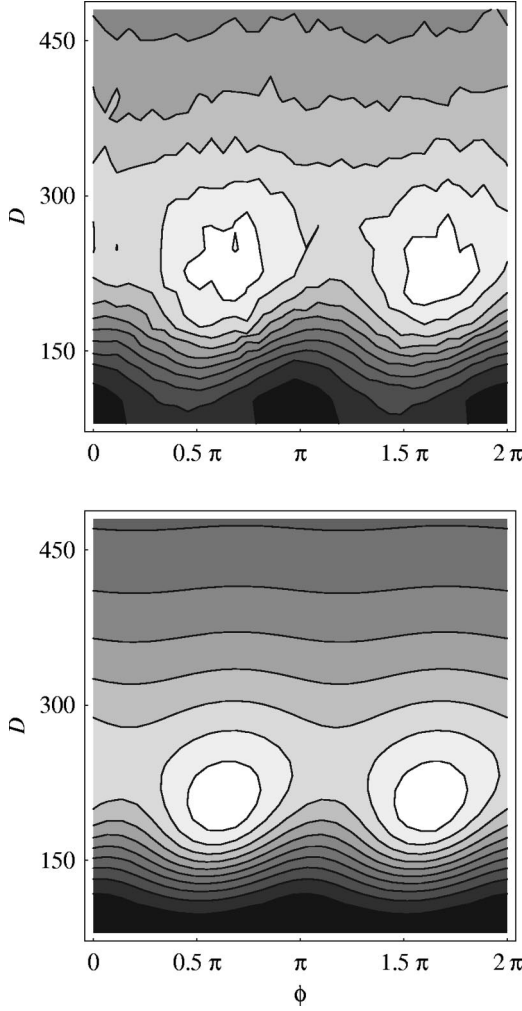


FIG. 11. Output signal power vs input noise strength  $D$  and phase  $\phi$  for the double well system with  $\omega_M = \omega_S$ . Parameters are as in Fig. 10. There is excellent agreement between the simulations (top) and the analytic predictions (18) (bottom). The gray scale range is (0,10).

$$\frac{\sqrt{\pi}}{k} \alpha_2 = \frac{e^{2\mu^2} \tilde{\phi}(\mu)^2}{\left( \int_{-\mu}^{\mu} e^{u^2} \phi(u) du \right)^3} - \frac{e^{\mu^2} \mu [\phi(-\mu) + \phi(\mu)]}{\left( \int_{-\mu}^{\mu} e^{u^2} \phi(u) du \right)^2},$$

$$\frac{\sqrt{\pi}}{k} \alpha_3 = \frac{e^{3\mu^2} \tilde{\phi}(\mu)^3}{\left( \int_{-\mu}^{\mu} e^{u^2} \phi(u) du \right)^4}$$

$$- \frac{2\mu e^{2\mu^2} \tilde{\phi}(\mu) [\phi(-\mu) + \mu \phi(\mu)]}{\left( \int_{-\mu}^{\mu} e^{u^2} \phi(u) du \right)^3}$$

$$+ e^{\mu^2} \frac{(2\mu^2 + 1) \tilde{\phi}(\mu) + 4\mu \phi'(\mu) + \phi''(\mu)}{3 \left( \int_{-\mu}^{\mu} e^{u^2} \phi(u) du \right)^2}, \quad (29)$$

where  $\phi(\mu)$  is the probability integral

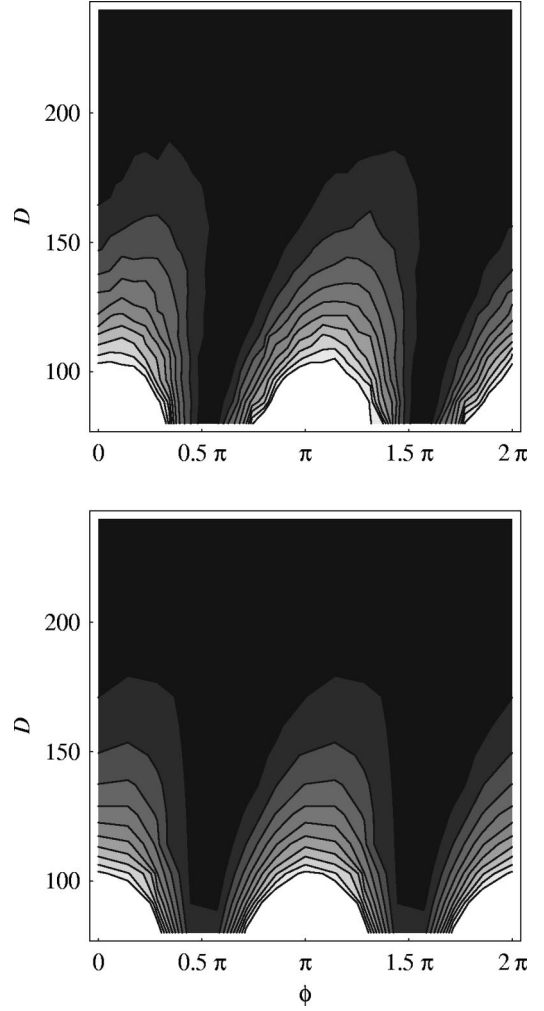


FIG. 12. Average dc output vs phase  $\phi$  and input noise strength  $D$  in the case of equal frequency modulation for the Duffing system (21). Parameters are the same as in Fig. 11. The top panel shows data from numerical simulations; the bottom panel displays the prediction (20). The dependence on  $D$  is implicitly defined via the expressions for the expansion coefficients (27). The gray scale range is (0,300).

$$\phi(\mu) = \frac{1}{\sqrt{\pi}} \int_{-\infty}^{\mu} e^{-u^2} du \quad \left( \Rightarrow \phi'(\mu) = \frac{1}{\sqrt{\pi}} e^{-\mu^2} \right.$$

$$\left. \text{and } \phi''(\mu) = \frac{-2\mu}{\sqrt{\pi}} e^{-\mu^2} \right)$$

and

$$\tilde{\phi}(\mu) = \phi(\mu) - \phi(-\mu) = \frac{1}{\sqrt{\pi}} \int_{-\mu}^{\mu} e^{-u^2} du.$$

[Expressions for the first two coefficients can be found in Eqs. (6.13) in [8].]

Using the notation of Sec. III, we let  $\mu = \gamma\sqrt{k}/\sigma$ ,  $\eta_S = -\epsilon_S\sqrt{k}/\sigma$ , and  $\eta_M = -\epsilon_M\sqrt{k}/\sigma$ . In order to obtain a qualitative agreement with the experimental results from Fig. 8, we replaced the parameters in Eqs. (29), (18), and (17) by their actual experimental values but for  $\epsilon_S$  and  $\epsilon_M$ , which

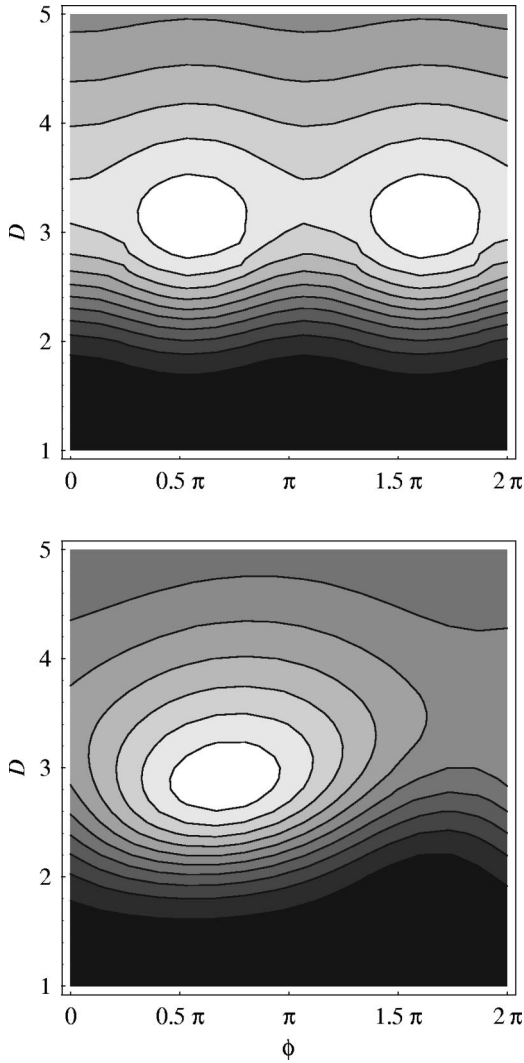


FIG. 13. Theoretical output signal power vs noise power  $D$  and phase  $\phi$  using the expressions (29) for the  $\alpha_n$ . Equation (18) is displayed in the top panel, Eq. (17) in the bottom panel. Parameters are as follows:  $k=10$  kHz,  $\gamma=300$  mV/9 V =  $\frac{1}{30}$ ,  $c=9$ ,  $\omega=2\pi 64$  s $^{-1}$ ,  $\epsilon_S=1/3000$ ,  $\epsilon_M=1/450$ . Notice that the experimental values  $\epsilon_S^{\text{exp}}=30$  mV/9 V =  $10\epsilon_S$ , and  $\epsilon_M^{\text{exp}}=200$  mV/9 V =  $10\epsilon_M$  are larger by a factor of 10. The qualitative agreement with the experimental results from Figs. 8(b) and 8(c), respectively, is excellent.

are chosen smaller (by a factor of 10) in order to stay within the perturbation theory approximation. The relatively large barrier modulation ( $A_M=200$  mV) in the experiment is beyond the low-order expansion. Figure 13 displays the theoretical results (18) and (17), respectively, utilizing the numerically computed  $\alpha_n$  given in Eq. (29). The analytical results agree qualitatively with the experimental results presented in Sec. II.

## V. SUMMARY

To summarize, we have developed a general theoretical framework for stochastic resonance in threshold-and-barrier-modulated bistable systems. The two-state theory successfully describes the low-order effects of a general nonfeedback control scheme, which can both enhance the

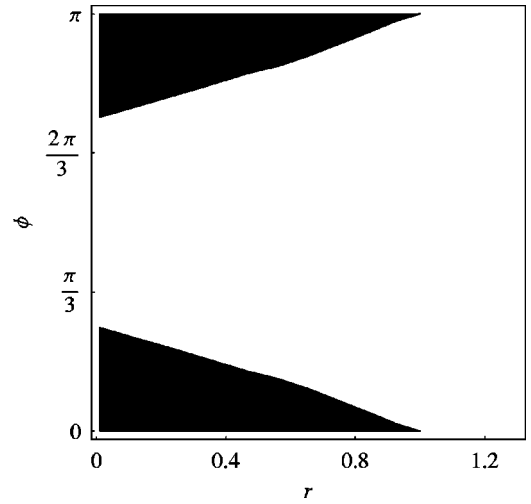


FIG. 14. Visualization of the region on parameter space for which  $[d_u^{\text{eff}}(t)]''|_{t_u} > 0$  and  $[d_l^{\text{eff}}(t)]''|_{t_l} > 0$  as a function of the ratio  $r=A_S/A_M$  and phase shift  $\phi$ . Both quantities are positive in the white region, while one of the two is negative in the black region. Note that the minima in the distances disappear for small values of  $r$ , i.e., if  $A_S \ll A_M$ .

“classical” SR effect and also suppress the response to a weak signal. Experiments were carried out on a generic stochastic resonator (a modified Schmitt trigger). Our experimental results are confirmed in computer simulations of the Schmitt trigger as well as in a potential double-well system. Within a range of signal and modulation amplitudes, the theory predicts the optimum phase difference and noise strength for maximum enhancement or suppression of the output signal power. The theory also shows good agreement with secondary effects, such as the dc offset for equal frequency modulation as well as a frequency dependent “drift” of the peak signal power for higher noise power. The good agreement found in our studies suggests that application of the theory to bistable systems other than the double well and the Schmitt trigger should work equally well. The key ingredient in any particular example is a knowledge of the transition rates, which could either be determined from first principles or directly measured.

We believe that controlled SR may be useful in applications as diverse as the cancellation of power-line frequencies in very sensitive magnetic sensing applications with superconducting quantum interference devices (SQUIDs) and vibration control in nonlinear mechanical devices, as well as in the context of electromagnetic field interactions with neuronal tissue [6], where control of internal thresholds is possible [12] and the selective suppression of specific frequencies could potentially be beneficial. Future work will aim to develop analytical expressions for the background noise power and also address the interesting case of incommensurate frequencies.

## ACKNOWLEDGMENTS

We acknowledge support from the Office of Naval Research, the Internal Research Program at SPAWAR Systems Center San Diego, the Deutsche Forschungsgemeinschaft (P.H.; Grant No. HA1517/18), and a NICOP grant (L.G.)

from ONR-Europe. M.L. would like to thank Anne-Katherina Jappsen for valuable technical help.

#### APPENDIX: EXISTENCE OF MINIMUM BARRIER DISTANCE

For  $\omega_M = \omega_S$ , the ‘‘distance’’ between the signal and the (modulated) threshold

$$\begin{aligned} d(t) &= d_u(t) = b + A_M \sin(\omega_S t + \phi) - A_S \sin \omega_S t \\ &\quad \text{if } 0 \leq \omega_S t \leq \pi \\ &= d_l(t) = b + A_M \sin(\omega_S t + \phi) + A_S \sin \omega_S t \\ &\quad \text{if } \pi \leq \omega_S t \leq 2\pi \end{aligned} \quad (\text{A1})$$

depends on the four parameters  $b, A_M, A_S$ , and  $\phi$ . If one is only interested in the existence of a minimum during the up and the down cycle, one can eliminate the offset  $b$  and rewrite Eq. (A1) as

$$\begin{aligned} d^{\text{eff}}(t) &= d_u^{\text{eff}}(t) = \sin(\omega_S t + \phi) - r \sin \omega_S t \quad \text{if } 0 \leq \omega_S t \leq \pi \\ &= d_l^{\text{eff}}(t) = \sin(\omega_S t + \phi) + r \sin \omega_S t \quad \text{if } \pi \leq \omega_S t \leq 2\pi, \end{aligned} \quad (\text{A2})$$

where  $d^{\text{eff}} = (d - b)/A_M$  depends on only two parameters, namely the phase  $\phi$  and the amplitude ratio  $r = A_S/A_M$ . To find the minimum distances we set  $(d_u^{\text{eff}})' = 0$  on the interval  $\omega_S t_u \in [0, \pi]$  and  $(d_l^{\text{eff}})' = 0$  on the interval  $\omega_S t_l \in [\pi, 2\pi]$ ,

respectively. Here, the prime denotes differentiation with respect to time. We find

$$\begin{aligned} \omega_S t_u &= \arccos\left(-\frac{\sin \phi}{\sqrt{r^2 - 2r \cos \phi + 1}}\right), \\ \omega_S t_l &= -\arccos\left(-\frac{\sin \phi}{\sqrt{r^2 + 2r \cos \phi + 1}}\right). \end{aligned}$$

It can happen that one of these extrema is actually a maximum. The intuitive arguments in Sec. III C about the resulting dc offset are meaningless unless the distance takes on a minimum in *both* partitions of the drive cycle, so we must check the second derivatives as well. These extrema are minima only if the second derivatives are greater than zero. The result is depicted in Fig. 14. Note that the role of  $\omega_S$  is merely to scale the time axis, i.e., it determines the location of the minima in time but not their existence. Figure 14 thus depends only on two parameters, the phase  $\phi$  and the ratio  $r$ . The black regions show the parameter combinations for which one of the extrema is a maximum; the white regions are where both  $[d_u^{\text{eff}}(t)]''|_{t_u}$  and  $[d_l^{\text{eff}}(t)]''|_{t_l}$  are positive. The figure reflects the fact that for small enough values of the ratio  $A_S/A_M$ , one of the minima in the up- and down-partition of the drive cycle changes into a maximum over a range of phase values. This is in contrast to the unmodulated case ( $A_M = 0$ ) where a minimum always exists and is well defined.

- 
- [1] R. Benzi, A. Sutera, and A. Vulpiani, *J. Phys. A* **14**, L453 (1981); C. Nicolis and G. Nicolis, *Tellus* **33**, 225 (1981).
- [2] For reviews see K. Wiesenfeld and F. Moss, *Nature (London)* **373**, 33 (1995); A. Bulsara and L. Gammaitoni, *Phys. Today* **49**(3), 39 (1996); L. Gammaitoni, P. Hänggi, P. Jung, and F. Marchesoni *Rev. Mod. Phys.* **70**, 223 (1998). An extensive bibliography can be found at <http://www.pg.infn.it/sr>
- [3] M. Stemmler, *Network* **7**, 687 (1996); A. Bulsara and A. Zador, *Phys. Rev. E* **54**, 2185 (1996); C. Heneghan *et al.*, *ibid.* **54**, R2228 (1996); A. Neiman *et al.*, *Phys. Rev. Lett.* **76**, 4299 (1996); F. Chapeau-Blondeau, *Phys. Rev. E* **55**, 2016 (1997); J. Robinson *et al.*, *Phys. Rev. Lett.* **81**, 2850 (1998).
- [4] J. Collins *et al.*, *Phys. Rev. E* **52**, R3321 (1995); *Nature (London)* **376**, 236 (1995); J. Levin and J. Miller, *ibid.* **380**, 165 (1996); D. Chialvo *et al.*, *Phys. Rev. E* **55**, 1798 (1997); L. Gammaitoni, *ibid.* **52**, 4691 (1995).
- [5] L. Gammaitoni, M. Löcher, A.R. Bulsara, P. Hänggi, J. Neff, K. Wiesenfeld, W.L. Ditto, and M.E. Inchiosa, *Phys. Rev. Lett.* **82**, 4574 (1999).
- [6] For reviews see, e.g., L.A. Sagan, *Electric and Magnetic Fields: Invisible Risks?* (Gordon and Breach, Amsterdam, 1996); T. Akerstedt, B. Arnetz, G. Ficca, and P. Lars-Eric, *J. Sleep Res.* **26**, 260 (1997). Review report by the National Institute of Health, available at [http://www.niehs.nih.gov/emfrapid/html/EMF\\_DIR\\_RPT/Report\\_18f.htm](http://www.niehs.nih.gov/emfrapid/html/EMF_DIR_RPT/Report_18f.htm).
- [7] S. Fauve and F. Heslot, *Phys. Lett.* **97A**, 5 (1983).
- [8] B. McNamara and K. Wiesenfeld, *Phys. Rev. A* **39**, 4854 (1989).
- [9] J.W.S. Rayleigh, *The Theory of Sound* (Dover, New York, 1945), Vol. 2, Chap. 23.
- [10] A. Grigorienco, P. Nikitin, and V. Roshchepkin, *Zh. Éksp. Teor. Fiz.* **85**, 628 (1997) [*JETP* **85**, 343 (1997)].
- [11] P. Jung and P. Hänggi, *Europhys. Lett.* **8**, 505 (1989); *Phys. Rev. A* **44**, 8032 (1991).
- [12] B.J. Gluckman *et al.*, *J. Neurophysiol.* **76**, 4202 (1996); *Phys. Rev. Lett.* **77**, 4098 (1996).
- [13] A complete derivation of the two cases  $\omega_M = 2\omega_S$  and  $\omega_M = \omega_S$  can be supplied by request or downloaded from the following Internet address: <http://www.physics.gatech.edu/people/faculty/markus/CSR/>. See also EPAPS Document No. E-PLLEE8-62-170007 for a comprehensive derivation of Expressions (15), (18), and (20) in the form of Mathematica Notebooks. The Mathematica documents can be viewed using MathReader (<http://www.wolfram.com/products/mathreader/>) without having to purchase Mathematica. This document may be retrieved via the EPAPS homepage (<http://www.aip.org/pubservs/epaps.html>) or from <ftp.aip.org> in the directory `/epaps/`. See the EPAPS homepage for more information.